Formation of second-generation stars in globular clusters

F. Calura [1]★ A. D'Ercole,[1] E. Vesperini,[2] E. Vanzella[1] and A. Sollima[1]

[1]*INAF - OAS, Osservatorio di Astrofisica e Scienza dello Spazio di Bologna, via Gobetti 93/3, I-40129 Bologna, Italy*
[2]*Department of Astronomy, Indiana University, Bloomington, IN 47401, USA*

ABSTRACT

By means of grid-based, 3D hydrodynamical simulations we study the formation of second-generation (SG) stars in a young globular cluster (GC) of mass $10^7\,\mathrm{M_\odot}$, the possible progenitor of an old GC with present mass $\sim(1\text{–}5)\times10^6\,\mathrm{M_\odot}$. The cluster accretes external gas as its first generation (FG) asymptotic giant branch (AGB) stars release their ejecta and SG stars form. We consider two models characterized by different densities of the external gas. In both cases, we find that a very compact SG subsystem with central density $>10^5\,\mathrm{M_\odot\,pc^{-3}}$ forms in the innermost regions of the cluster. The low-density model forms a population of extreme SG stars with high helium enhancement, followed by the formation of another SG group out of a mix of pristine gas and AGB ejecta and characterized by a modest helium enhancement. On the other hand, the high-density model forms in prevalence SG stars with modest helium enhancement. Our simulations illustrate the dynamical processes governing the formation of SG populations in GCs and shed light on the structural properties emerging at the end of this phase. The newly born SG groups have different concentrations, with more extreme SG stars more centrally concentrated than those with less extreme chemical abundances. The very high density of the SG subsystems implies that SG massive stars, if formed, might suffer frequent close encounters, collisions, and gas stripping, thus possibly contributing further gas to the SG formation.

Key words: hydrodynamics – methods: numerical – globular clusters: general – galaxies: star formation.

1 INTRODUCTION

In the last decades, strong evidence of the presence of multiple stellar populations has been found in all the Galactic globular cluster (GCs) that have been investigated by means of photometric or spectroscopic studies.

Many spectroscopic studies revealed that GCs host stellar populations that are not chemically homogeneous; even if GC stars are generally homogeneous in their Fe content, they are characterized by significant star-to-star abundance variations in a number of light elements, such as C, N, O, Na, Mg, Al (see e.g. Gratton, Sneden & Carretta 2004; Carretta et al. 2009a, 2009b; Gratton, Carretta & Bragaglia 2012, and references therein). More recently, high-precision photometric observations have provided further evidence in support of the presence of multiple stellar populations in GCs (see e.g. Lee et al. 1999; Bedin et al. 2004; Ferraro et al. 2004; Piotto et al. 2005, 2007, 2015; Marino et al. 2008; Milone et al. 2017, for a review, see Gratton et al. 2012; Bastian & Lardo 2018).

Despite the wealth of observational data collected so far, our current understanding of the origin of multipopulations in GCs is still incomplete. Several models have been proposed so far, none of which is free from drawbacks and assumptions invoking complex physical conditions sometimes difficult to test. One of the most thoroughly studied model is the asymptotic giant branch (AGB) scenario, in which a second generation (SG) of stars forms from the ejecta of first-generation (FG) AGB stars (e.g. D'Ercole et al. 2008, 2010, 2012; D'Antona et al. 2016). Other scenarios proposed so far include models in which SG stars form from gas processed in fast-rotating massive stars (Decressin et al. 2007), massive interacting binaries (de Mink et al. 2009), black hole accretion discs (Breen 2018), massive (Elmegreen 2017), or even supermassive ($M > 10^3\,\mathrm{M_\odot}$) stars (Denissenkov & Hartwick 2014; Gieles et al. 2018). All scenarios need to face a variety of complex observational constraints concerning, for example, the chemical properties of multiple populations, the number of populations, the relative number of FG and SG stars, as well as their dynamical properties. One of the constraints often discussed in the literature concerns the initial mass of the FG cluster needed to produce the observed number of SG stars. All the possible sources of processed gas for the SG formation proposed in the literature do not release large quantities of gas and, to account for the fraction of SG stars observed in GCs today, it is therefore necessary to assume that the mass of the GC precursors had to be initially larger than present-day clusters.

★ E-mail: francesco.calura@inaf.it

The hydrodynamical study presented here is conducted within the AGB scenario and extends the early exploration by D'Ercole et al. (2008). By means of 1D hydro simulations, D'Ercole et al. (2008) showed that the AGB ejecta collects in a cooling flow leading to the formation of a more centrally concentrated SG subsystem in the central regions of the primordial cluster. Several observational studies have found clusters in which some memory of this initial spatial difference is still retained and in which the SG is more spatially concentrated than the FG (see e.g. Sollima et al. 2007; Bellini et al. 2009; Lardo et al. 2011; Milone et al. 2012; Simioni et al. 2016). The possible origin of the chemical abundances of elements such as Na, O, Al, Mg, Li in multiple population clusters have been extensively studied in the AGB scenario (see e.g. D'Ercole et al. 2010, 2012; D'Antona et al. 2016; D'Antona et al. 2019) along with the possible origin of discrete groups in the SG populations. We refer to those papers for a detailed discussion of the uncertainties and the various constraints and open questions concerning the AGB stellar models nucleosynthesis. A problematic aspect pointed out in these studies concerns the fact that in order to account for the chemical composition of GC stars, in particular the pattern followed by light elements, the AGB scenario must invoke dilution of AGB ejecta with pristine gas occurring during SG formation. A similar requirement of dilution with pristine gas is shared by other models (see e.g. Decressin et al. 2007; Denissenkov et al. 2015; Gieles et al. 2018). The requirement of pristine gas in the mix out of which SG stars form opens a new fundamental question concerning the hydrodynamics of this gas during the SG formation and provides the main motivation for the study presented in this paper. An additional problem which is briefly discussed in this paper but which will require further exploration in future studies concerns the possible role of feedback of SG massive stars and other energy sources.

Despite the general consensus regarding the need for dilution, the source of the diluting pristine gas is still not clear, and all the mechanisms proposed so far (Bekki & Mackey 2009; Pflamm-Altenburg & Kroupa 2009; D'Ercole et al. 2010; Gratton & Carretta 2010; Conroy & Spergel 2011; D'Ercole, D'Antona & Vesperini 2011; D'Ercole, D'Antona & Vesperini 2016) require further explorations of the gas dynamics and the implications for the resulting abundance patterns.

Because of the complexity and the variety of the physical processes involved in the accretion process, an analytic estimate of the mass of external gas accreted by a cluster is problematic. While for a point mass accretor the mass accretion rate can be estimated by means of the Bondi–Hoyle–Lyttleton formula (Bondi 1952), an analogous simple analytical formula for the accretion on to potentials for extended mass distributions is not available, and one must therefore resort to numerical simulations. A significant step forward in this field is represented by the work of Naiman, Ramirez-Ruiz & Lin (2011; see also Kaaz, Antoni & Ramirez-Ruiz 2019), who performed a set of numerical simulations appropriate for different astrophysical contexts. Naiman et al. (2011) modelled the accretion on to various core potentials (e.g. of the Plummer- and Hernquist-type) moving through a background medium, as example studies of various astrophysical environments, including gas accretion on to star clusters. The results of their simulations shed light on a number of key aspects of the accretion process although they still invoke a few important simplifications, in that mass return from cluster stars, the self-gravity of the gas, and star formation (SF) are not included. The simulations of Naiman et al. (2011) show that, in general, the accumulation of external gas occurs during an initial period lasting between ~10 and 100 sound crossing times of the

cluster. Their results indicate that eventually a steady configuration is established, and the gas accumulated into the cluster ceases to grow appreciably. According to their results, the gas accumulated into the core may reach very high densities and, since the local free-fall time is very short, new stars could, in principle, form rather quickly. Although this is a very promising result as it suggests that the cluster can indeed re-accrete the correct amount of needed pristine gas (see e.g. D'Ercole et al. 2010, 2011, 2012, 2016), in order to have a more realistic physical description of a proto-GC, additional simulations are necessary. In particular it is important to consider simulations combining the mass return from AGB stars, the accretion of pristine gas, the gas self-gravity as well as the formation of SG stars, four ingredients which have never been simultaneously taken into account in previous numerical studies of GC formation.

In this paper, we present for the first time three-dimensional hydrodynamic simulations of a star-forming GC which includes all such ingredients. In particular, we investigate various aspects related to the formation and early evolution of a GC in the framework of the AGB scenario presented in D'Ercole et al. (2016). In our simulations, the GC moves through a distribution of external gas and is allowed to accrete mass from it.

Although the set-up is still idealized, our numerical experiments are designed to provide a well-controlled, theoretical framework which includes several key ingredients for the formation of SG stars in a young GC. We point out that the main goal of the paper is to address a very specific question concerning the possible re-accretion of the pristine gas, explore the dynamics of multiple population formation from this pristine gas and AGB ejecta, and the emerging structural properties of the multiple population subsystems. Many different aspects concerning the chemical and dynamical evolution of multiple populations, which are beyond the scope of this investigation, remain to be further studied. Moreover it will be important to extend the study of the hydrodynamics of the SG formation in the context of the various other scenarios proposed in the literature and further explore their signatures in the present-day chemical and structural properties of GCs (see e.g. Bekki 2019; Howard et al. 2019).

This paper is organized as follows: in Section 2 we present our model, in particular the set-up of our hydro simulation and describe our most crucial assumptions. In Section 3, we present our results and in Section 4 we discuss their most important implications and future directions. Finally, in Section 5 we draw our conclusions.

2 SIMULATION SET-UP

In this work, the initial conditions coincide with the final stage of the simulations presented in Calura et al. (2015), although some of the model parameters are different. In our initial set-up, the stellar FG is $\sim t_{\mathrm{AGB}} = 39$ Myr old. At this time, all FG type II Supernovae (SNe) have exploded, no primordial gas or supernova (SN) ejecta are left in the cluster, and the most massive FG AGBs are starting to return mass and energy into the gas-free system.

As discussed in Section 1, previous studies have shown that the SG cannot form out of AGB ejecta only, as the observed abundance pattern followed by light elements would not be reproduced without a certain amount of dilution from pristine gas (i.e. not polluted either by FG SNe or by AGB stars; see e.g. D'Ercole et al. 2011; Bastian, Cabrera-Ziri & Salaris 2015).

Our numerical simulations are designed to describe the motion of a cluster with respect to a background gas distribution. Starting from a given time $t_w > t_{\mathrm{AGB}}$, pristine gas starts to flow inside our
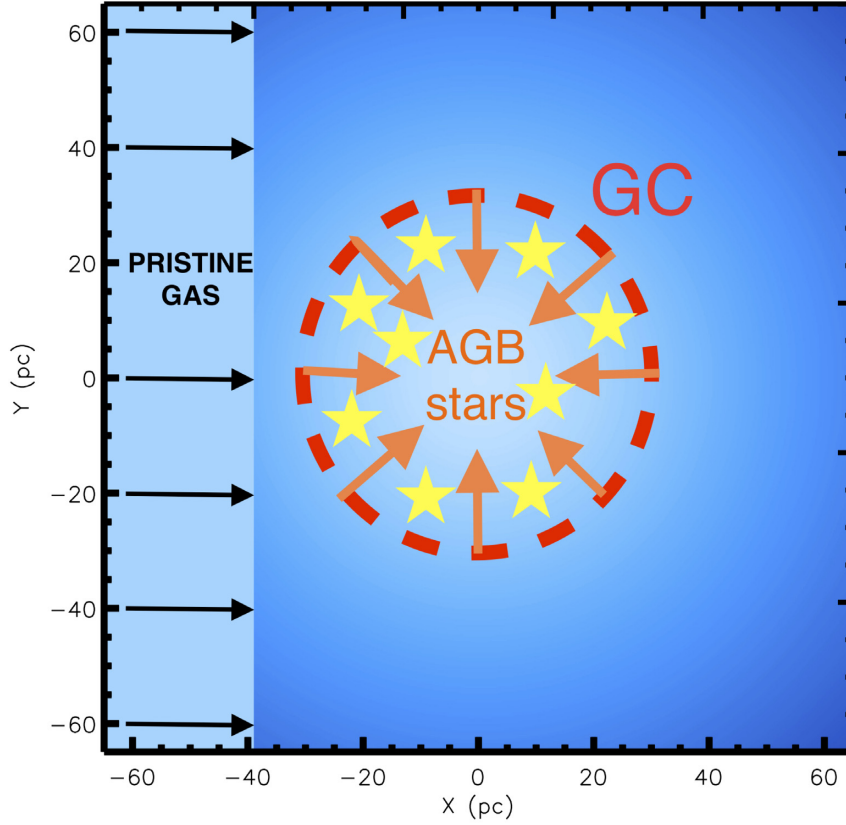
Figure 1. A schematic description of the set-up of our simulation. At the beginning of our simulation, corresponding to $t \sim 40$ Myr after the birth of the cluster, FG AGB stars start releasing their ejecta and SG stars can form out of this gas. Starting from a given time t_w, a uniform pristine gas distribution with the same chemical comoposition as FG stars enters the computational box from one of the boundaries.

computational box from one of the boundaries. In principle, this set-up is designed to recreate the physical conditions described in D'Ercole et al. (2016), in which the GC is assumed to lie within the disc of a galaxy at high redshift (Kravtsov & Gnedin 2005; Kruijssen 2015). However, the gas distribution may also represent other real cases such as, e.g. a reservoir of gas leftover from a merger, and the motion could also describe a newly born cluster orbiting around the centre of a dwarf galaxy or migrating towards it (Goodman & Bekki 2018).

Following D'Ercole et al. (2016), assuming that the FG type II SNe carved a large cavity into the external gas distribution and that the FG cluster is moving along it, the system would experience an asymmetric re-accretion of gas from the side towards which the cluster is moving.

In order to create such a condition, for the purposes of simplicity, we assume a reference frame in which the cluster is at rest, and we assume that it is accreting mass from one of the boundaries, as shown in Fig. 1.

For the computation of t_w, we follow D'Ercole et al. (2016). For a cluster in motion with respect to the ISM, the radius at which the ram pressure due to the supernova-driven wind balances the pressure of the external medium can be computed as:

$$R_{eq}[100 \text{ pc}] = 41.43 \left(\frac{L_{41}}{n_0 \, V_{w,8} \, (\sigma_{0,6}^2 + v_{pg,6}^2)} \right)^{\frac{1}{2}}. \quad (1)$$

The quantity L_{41} is the mechanical luminosity of the wind in units of 10^{41} erg s^{-1}, whereas $V_{w,8} \sim 2$ is the velocity of the wind in

units of 10^8 cm s^{-1}. For a cluster of mass $M_{FG} = 10^7$ M$_\odot$ and for a standard stellar initial mass function (IMF; i.e. Kroupa 2001; Chabrier 2003), we have $\sim 10^5$ SNe and $L_{41} \sim 1$. The two terms $\sigma_{0,6} \sim 1$ and $v_{pg,6} = 2$ are the isothermal sound speed and the velocity of the pristine gas relative to the GC (both in units of 10^6 cm s^{-1}), respectively, whereas n_0 is the gas density in cm^{-3}. The time at which the infall starts can then be computed as

$$t_w = t_{SN} + \frac{R_{eq}}{\sigma_0 + v_{pg,6}}, \quad (2)$$

where $t_{SN} \sim 30$ Myr is the time after which all FG type II SNe have exploded. Assuming $V_{w,8} \sim 2$ and $n_0 \sim \rho_{pg}/m_p$ (where m_p is the proton mass), we obtain $t_w \sim 60$ Myr and $t_w \sim 40$ Myr for $\rho_{pg} = 10^{-24}$ g cm^{-3} and $\rho_{pg} = 10^{-23}$ g cm^{-3}, respectively.

The cluster is assumed to move with respect to the external uniform gas distribution, with a velocity of the order of the isothermal sound speed of a medium characterized by a temperature of $\sim 10^4$ K (see Section 2.2.1). We point out that the computation of t_w requires assumptions regarding several uncertain parameters, including the cluster velocity with respect to the ISM, the SN mechanical luminosity, and the efficiency with which SN energy is deposited in the ISM, the motion of the cluster with respect to the external gas distribution, the clumpiness of the medium, or the possible presence of density gradients. For these reasons, we regard the value computed above for t_w as representative order-of-magnitude estimate. A summary of the main parameters describing the two models considered here is presented in Table 1.

Table 1. Parameters describing the simulation set-up.

Parameter	Description	Adopted values
ρ_{pg}	Density of pristine gas	$10^{-23}; 10^{-24}\,\mathrm{g\,cm^{-3}}$
$v_{pg,6}$	Pristine gas velocity	$20\,\mathrm{km\,s^{-1}}$
T_{pg}	Temperature of the pristine gas	$10^4\,\mathrm{K}$
T_{floor}	Minimum temperature of the simulations	$10^3\,\mathrm{K}$
t_*	Star formation time-scale	$0.1\,\mathrm{Gyr}$
M_{FG}	Mass of FG stars	$10^7\,\mathrm{M_\odot}$
r_{Plum}	Plummer radius of FG stellar distribution	$23\,\mathrm{pc}$
t_{end}	Duration of SG star formation	$65\,\mathrm{Myr}$

We performed several low-resolution tests in which we varied the basic parameters describing the flow of matter on to the cluster. In particular, attempts carried on with a density of the infalling medium by more than one order of magnitude larger than the one assumed here (i.e. $>10\,\mathrm{cm^{-3}}$ or more) provided negative results for the capability of the system to retain the gas, in that SG stars were originating in a loose, unbound structure rapidly dissolved by the flow, and hence could not aggregate into a bound core. A similar outcome was obtained assuming a flow velocity much larger than the value adopted here, which roughly corresponds to the double of the isothermal sound speed of a gas at $\sim 10^4\,\mathrm{K}$. In fact, as also shown by a few previous studies, in such conditions an efficient accretion may work only for a limited range of values of the parameters of interest. If the energy of the incoming gas is much larger than the GC potential well, a collective accretion is prevented. Moreover, if the cluster velocity is too large, the ram pressure exerted on the gas at the bottom of the potential well becomes stronger than the gravitational restoring force, and the sweeping process clears out the cluster of its gas instead of promoting accretion (Mori & Burkert 2000; Lin & Murray 2007; Conroy & Spergel 2011).

The physical conditions of the infalling material in the simulations on which this paper is focused, which are reported in Table 2, are not far from those observed in real systems, such as the gas density in a dwarf galaxy (Marcolini, Brighenti & D'Ercole 2003, and references therein) or in a high-redshift disc (D'Ercole et al. 2016; Wardlow et al. 2017).

2.1 Main physical ingredients

In this work, we use a customized version of the RAMSES hydrocode (Teyssier 2002) to study SF occurring within a young GC by means of 3D hydrodynamic simulations. Besides mass and energy return from AGB stars, our model also includes radiative cooling and SF. The gravitational effects of FG and SG stars and the self-gravity of the gas are taken into account, along with the chemical composition of the stellar ejecta and of newly formed stars. In this section we describe the main ingredients of our hydrodynamic simulations. The total, cubic computational volume is $L_{box}^3 = 160^3\,\mathrm{pc^3}$. Our simulations are run using a uniform grid, with maximum resolution equal to $\sim 0.3\,\mathrm{pc}$. The gas evolution is computed using a second-order Godunov scheme for the Euler equations. Collisionless star particles are allowed to form, and their trajectories are computed by means of a particle-mesh solver.

The gravitational effects of FG stars are taken into account by means of a static potential, computed from their density profile (equation 5). The self-gravity of the entire system composed by SG stellar particles and gas is fully taken into account, and these two components do exert gravitational force on each other and are subject to the effects of FG stars.

2.2 Mass, energetic, and chemical feedback from AGB stars

Mass return from AGB stars is modelled by adding a source term to the mass conservation equation, representing the rate of mass return per unit volume and expressed as:

$$\dot{\rho}_{*,AGB} = \alpha \rho_*, \tag{3}$$

where ρ_* is the stellar density of FG stars. The quantity α is the specific mass return rate and is computed following the formalism of Ciotti et al. (1991) (see their equation 3) adopting a universal IMF (Kroupa 2001). If t_{yr} represents the time expressed in yr, the quantity α as a function of time (expressed in $\mathrm{yr^{-1}}$) is represented by the analytical formula

$$\alpha(t_{yr}) = 0.065 \times t_{yr}^{-1.01}. \tag{4}$$

The formula is valid for times between 30 and 100 Myr.

FG stars follow a Plummer (1911) mass density profile:

$$\rho_*(r) = \frac{3M_{tot}}{4\pi\,a^3}\left(1 + \frac{r^2}{a^2}\right)^{-\frac{5}{2}}, \tag{5}$$

with $M_{tot} = 10^7\mathrm{M_\odot}$ and $a = 23\,\mathrm{pc}$ (corresponding to a half-mass radius equal to 30 pc). The mass chosen is meant to represent that of the possible progenitor of the most massive Galactic GCs (after mass-loss occurring during the cluster's early and long-term dynamical evolution is taken into account; see e.g. D'Ercole et al. 2008). We emphasize that the characteristic radius and the stellar mass for FG stars chosen here are very similar to the values observed in proto-GC candidates at $z \sim 3$ and $z \sim 6$, recently detected in gravitationally lensed fields (Vanzella et al. 2017a, b).

We emphasize that the stellar mass of the FG enclosed within the computational box adopted for the simulations includes $\sim$ 90 per cent of M_{tot} and therefore for the purposes of calculations concerning the relative SG to FG mass in the rest of the paper, the mass of the FG system to be considered is equal to $0.9\,M_{tot}$ ($9 \times 10^6\,\mathrm{M_\odot}$).

The energetic input from FG AGB stars is taken into account by means of the source term:

$$S = 0.5\,\alpha\,\rho_*\,(3\sigma^2 + v^2 + v_{wind}^2), \tag{6}$$

where v is the fluid velociy, σ is the velocity dispersion, computed for a Plummer sphere following Dejonghe (1987), and $v_{wind} \sim 2 \times 10^6\,\mathrm{cm\,s^{-1}}$ is the wind velocity for AGB stars (D'Ercole et al. 2008). The source term S represents the heating of the gas due to the feedback from FG AGB stars and is added at each time step to the fluid energy.

2.2.1 Thermal modelling

Besides heating from AGB stars, our simulations also include radiative gas cooling. The cooling function implemented in RAMSES takes into account H, He, and metal cooling (Sutherland & Dopita 1993, see Few et al. 2014). The contribution from metals at temperatures above $10^4\,\mathrm{K}$ is accounted for through a fit of the ratios between the cooling rates calculated at solar metallicity and those at zero metallicity using the photoionization code CLOUDY (Ferland et al. 1998).

At lower temperatures, metal line-structure cooling rates are from Rosen & Bregman (1995).

The temperature chosen for the external medium, i.e. the pristine gas which continuosly enters the computational box from one of the boundaries, is $10^4\,\mathrm{K}$. Such a temperature value is quite standard for

the interstellar medium of a 'normal', star-forming galaxy which is kept photoionized by a stable UV stellar radiation field (e.g. Haffner et al. 2009).

The temperature threshold for radiative cooling adopted in this work is 10^3 K, i.e. anywhere in the volume the gas is not allowed to cool down to a temperature below this value. This choice is motivated by the impossibility of resolving the Jeans length, which decreases with the minimum temperature, set by the temperature floor. With our assumption ($T_{\rm floor} = 10^3$ K) and with a density of $\sim 10^{-16}$ g cm^{-3} (the maximum achievable in clusters), the Jeans length is of the order of 0.01 pc (and it would be even smaller for a lower value of $T_{\rm floor}$), well below our maximum resolution. In general, in our simulations numerical convergence is satisfactory (see Fig. 6) and we do not find any 'density runaway', which sometimes may occur when the Jeans length is not well resolved (Truelove et al. 1997). Moreover, at very large densities, in principle a lower value for $T_{\rm floor}$ should not lead to strong variations in our results, as the cooling time is generally much lower than the Courant time, and the amount of gas that rapidly cools to form stars is not expected to change much.

Our simulations are aimed at roughly modelling a two-phase medium (i.e. a 'neutral' one, where SF can occur, and an 'ionized' ambient which surrounds the star-forming centre of the cluster). Our equation of state is $P \propto \rho^\gamma$, where P and ρ are the pressure and density of the gas, respectively, and $\gamma = 5/3$.

2.2.2 Star formation model

The SF model used in this work relies upon the native RAMSES SF implementation as described in detail in Rasera & Teyssier (2006).

In each cell eligible for SF, the gas can be converted into star particles and new stars with density $\rho_{*,\rm SG}$ can form according to:

$$\dot\rho_{*,\rm SG} = \frac{\rho}{t_*}, \tag{7}$$

i.e. according to the Schmidt (1959) law. In each cell, the SF time-scale t_* is proportional to the local free-fall time, and computed as

$$t_* = t_0 \left(\frac{\rho}{\rho_0}\right)^{-1/2}. \tag{8}$$

Here we have combined the unknown quantities t_0 and ρ_0 in order to have $t_* \sim 0.1$ Gyr for a density ρ of the order of one atom per cubic centimetre. However, our results do not depend significantly on the choices of the free parameters t_0 and ρ_0. As shown by D'Ercole et al. (2008), this is true when the replenishment of the gas occurs on time-scales which are much shorter than the time-scale of the simulation.

For numerical reasons, the code allows that no more that 90 per cent of the gas in the cell can be used for star particle formation. A single star particle is formed in each cell cooled down to a temperature $T < 2 \times 10^4$ K (i.e. where the gas is assumed to be neutral) and where the net flow is converging, i.e. in which

$$(\nabla \cdot \boldsymbol{v}) < 0, \tag{9}$$

where $\boldsymbol{v}$ is the fluid velocity in the cell.

The mass of each collisionless stellar particle is $M_{\rm p} = N\,m_0$, where $m_0 = 0.1$ M$_\odot$ is the minimum mass and N is determined by sampling from a Poisson distribution, characterized by a probability P given by

$$P(N) = \frac{\lambda_P^N}{N!} \exp(-\lambda_P), \tag{10}$$

where the mean value is calculated as:

$$\lambda_P = \left(\frac{\rho \Delta x^3}{m_0}\right) \frac{\Delta t}{t_*}. \tag{11}$$

In this equation Δt represents the time step, whereas Δx is the cell size.

These star particles are placed at the centre of their parent cell, with a velocity equal to the local fluid velocity. The corresponding mass, momentum, energy, and density in the form of the chemical element k are conservatively removed from the ones of the parent cell.

SF is halted after 65 Myr, corresponding to $t_{\rm AGB}$ + 65 Myr = 104 Myr after the formation of the FG. This choice for the duration of the SG SF event is determined by the uncertain time-scale of the explosions of the first FG Type Ia SNe. Our choice is consistent with the time-scales suggested by observational studies (see e.g. Mannucci et al. 2006; Maoz, Mannucci & Nelemans 2014) but is meant to provide just a general indication of the time-scale of the SG SF event. The implications of earlier explosions of SNIa are illustrated by the panels in Figs 3 and 5, showing the results at earlier times, whereas later SNIa explosions would further extend the SG SF episode possibly increasing the fraction of SG stars with very moderate chemical anomalies. A more extended SG formation would also imply a contribution of low-mass AGBs ($m < 5\,{\rm M}_\odot$) possibly producing SG populations with the s-process elements anomalies observed in some clusters (see e.g. D'Antona et al. 2016 for a further discussion). Energy release from SG massive stars, if they form, could provide another mechanism halting SG SF (see Section 4.1). We note that in the models presented in this paper SF is continuous, but in reality it could be more complex and characterized by separate SF bursts (see e.g. D'Antona et al. 2016 for a discussion of the possible role of delayed SNII events). Modelling SG SF including separate bursts, the detailed implications of different durations for the SF event, and the processes behind them is beyond the scope of this work and will be addressed in a future study.

Finally, as far as the chemical properties of SG stars formed are concerned, we follow only the evolution of the helium abundance. The helium abundances used in this work are those calculated in Ventura & D'Antona (2011; for the helium yield of the 8 M$_\odot$ progenitor we adopt a value approximately equal to the average of the yields of the model of Ventura & D'Antona 2011 and Siess 2010; see Ventura & D'Antona 2011), calculated for a metallicity $Z = 10^{-3}$. The focus of this study is only on the dynamics of SG formation and we will not go into any detailed characterization of the abundance patterns of other elements such as Na, O, C, N, Al, Mg. The study of the origin of the observed abundance pattern and the nucleosynthesis of the possible polluters has been the subject of many studies and is still the subject of intense and debated observational and theoretical investigations (see e.g. D'Ercole et al. 2010, 2012; Denissenkov & Hartwick 2014; Denissenkov et al. 2015; D'Antona et al. 2016). The high complexity of the questions concerning the chemical properties of SG stars clearly shows the need for further specific studies of this aspect of the multiple population phenomenon. In future studies we will expand our investigation to combine the dynamical study with the chemical aspects and address more specifically the possible origin of the observed abundance pattern for more chemical elements.

Finally, one note is in order regarding the chemical composition of the diluting material which mixes with the AGB ejecta when SF occurs. The composition of such gas is not expected to be significantly different from that of FG stars. If the GC is orbiting in a dwarf galaxy of metallicity $Z \sim 0.001$, the heavy element content of the gas encountered by the system is not likely to have changed
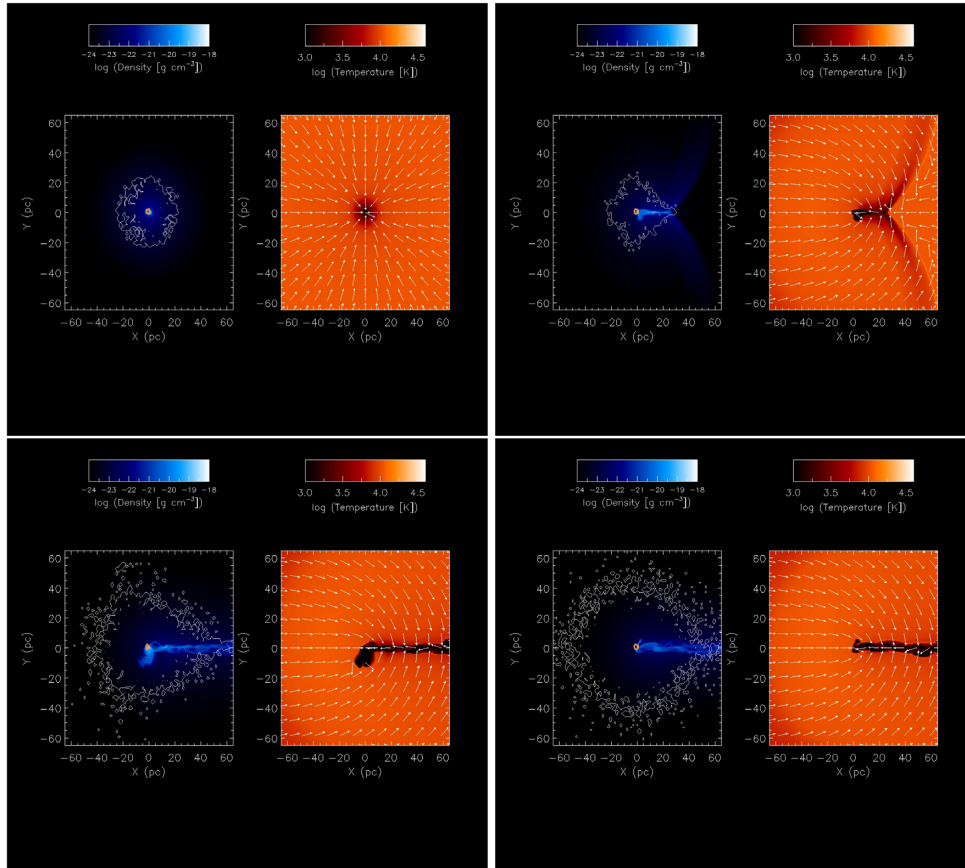
Figure 2. Two-dimensional gas density (left-hand panels of each plot, in black–blue–white colour scale) and temperature (right-hand panels, in black–orange–white colour scale) maps in the *x*–*y* plane in our low-density simulation at various time steps (from top-left, clockwise: 10, 26, 39, 63 Myr). The white arrows in the temperature maps represent the velocity field. The white and orange contours describe regions where the SG stellar density is $\geq 10^{-6}$ and ≥ 0.5 times the maximum value, respectively. The orange contours enclose large fractions (> 65 per cent) of the SG stellar mass.

much on a time-scale of 40 Myr. In fact, chemical evolution models for galaxies of different morphological types indicate that significant metallicity variations occur on rapid time-scales only in extremely metal-poor environments (e.g. Calura et al. 2009). Moreover, radial metallicity gradients in dwarf galaxies are typically of the order of ~0.1 dex kpc^{-1} (see e.g. El-Badry et al. 2016; Wang et al. 2019). This implies that, even in the extreme case in which the system was moving on a completely radial orbit with a speed of 20 km s^{-1}, the variation in metallicity would be of 0.08 dex, i.e. within the metallicity spread (as traced by [Fe/H]) of FG and SG stars in most GCs (e.g. Renzini et al. 2015). Clearly, a less extreme orbit spanning a smaller range of radial distances would lead to a smaller metallicity variation.

3 RESULTS

In this paper we present the results of models including the infall from a homogeneous, isothermal gas distribution; specifically, we focus our attention on a model in which the infalling gas has a density $\rho = 10^{-24}$ g cm^{-3}, and another with an infalling gas 10 times denser.

These two models provide an initial framework illustrating several key aspects of the dynamics of the SG formation and the link between the dynamics and the resulting SG chemical properties. In both cases, the general behaviour of the gas and of the newly born stellar population is first analysed by means of two-dimensional

density and temperatures maps for the gas distribution. For the purposes of clarity, for all the results presented in the remainder of the paper the times will be expressed assuming $t_{AGB} = 39$ Myr as the initial value (e.g. $t = 3$ Myr will correspond to $t_{AGB} + 3$ Myr = 42 Myr after the formation of FG stars). A more extended survey of models exploring different properties of the cluster and of the external environment will be matter for future studies.

3.1 Low-density model

3.1.1 Dynamical evolution of the gas

In Fig. 2, we show two-dimensional density and temperature maps computed at four different evolutionary times of the low-density model run. The maps have been calculated by selecting all the grids crossed by a plane centred at the middle of the computational volume and perpendicular to the *z*-axis. In this case, the evolutionary times are $t = 10$ Myr, $t = 26$ Myr, $t = 39$ Myr, and $t = 63$ Myr.

At 10 Myr, the system is still isolated in that the infall of pristine gas has still to start.

At this time, the ejecta of the AGB are giving rise to a cooling flow, directed towards the cluster core, where SG stars have begun to form. The cooling flow is visible from the velocity field of the gas in the top-left temperature map of Fig. 2, traced by the thin white arrows, all directed towards the centre of the cluster.

At the centre of the box, a cold condensation of gas is already visible, characterized by a temperature very close to T_{floor} (10^3 K). Such a condensation has purely formed out of the matter ejected by AGB stars and is characterized by a fairly regular, spherical shape. In the density map, the thin, white contour encloses the entire SG stellar mass in the x–y plane, computed considering a reference frame with an origin at the centre of the computational volume. As visible from the top-left density map, a small amount of stars has already formed at the very centre of such a condensation. The stellar component is extremely compact, as shown by the thick orange contour, which at this time encloses more than 90 per cent of the SG stellar mass in the plane.

At this time, the mass which has been turned into stars is $\sim 10^5$ M$_\odot$, and it consists of all the most extreme, He-rich stars representing the first SG stars ever formed.

At a later time ($t = 26$ Myr), the infall of pristine gas has already started, and the incoming shock front has just crossed the centre of the cluster. Upstream of the cluster, the velocity field reflects the motion of the incoming gas, in that the arrows appear aligned along the symmetry axis, and otherwise are tilted by the gravitational acceleration caused by the cluster itself, with an inclination gradually increasing along the y-axis and as the distance from the centre gets smaller and smaller. The symmetric, thin density enhancement caused by the shock is visible from the two 'wings' located at the right side of the cluster centre. This is caused by the distorted front of the shock, which appears warped into a sharp cusp pointing towards the centre. The interaction between the cold AGB ejecta and the shock has modified also the shape of the central cold condensation. This is visible from the drop-shaped, cold density enhancement visible at the centre of the x–y plane. The gas which composes such a structure and which lies in its short tail is directed towards the centre of the plane. Downstream of the cluster, the velocity field shows a hint of alignment perpendicular to the symmetry axis. On the right side of the plots and downstream of the shock, in a small part of the plane still unaffected by the shock, the velocity field still preserves its original features and points towards the cluster centre.

At later times ($t \sim 39$Myr), the shock has entirely crossed the cluster and a narrow, dense, and cold tail has emerged. Such a tail started to grow as the gas ram-pressure-stripped from the head of the bow shock was channelled behind the cluster centre. The tail is stretched downstream, and it appears as a noticeable overdensity extending along the direction of motion. This overdensity is the typical by-product of a massive perturber moving through a uniform medium and creating a density wake (e.g. Park & Bogdanovic 2017 and references therein for a recent study on the role of this density wake in case of dynamical friction in a gaseous medium).

The motion of the channelled matter flowing around the core is still outlined by the velocity field. The gas lying along the tail is accelerated towards the centre of the plane, i.e. the x-component of the velocity vector appears reverted with respect to the gas lying above and below the tail. Globally, the stellar distribution appears to follow the elongated shape of the gas flow, in that star particles are distributed and scattered around the cluster but tend to gather downstream along the tail, forming a drop-like shape. However, the stellar component is still strongly condensed in the very centre, as outlined by the thick, orange contours in the density map, which include the large majority of the stellar mass (for further detail, see the caption of Fig. 2).

At this stage, the tail has grown and evolved into an 'accretion column' (Bondi & Hoyle 1944; Shima et al. 1985; Moeckel & Troop

2009), through which matter can continuously flow on to the cluster and mix with the AGB ejecta.

The density appears to vary along the tail and its body is composed of several entangled, thin filaments. Inside the tail, the velocity field presents significant differences from the regular behaviour visible elsewhere in the plane. Globally, the motion of the cold gas composing to the tail is still directed towards the centre, but now it appears chaotic and turbulent, in particular by looking at the y-component of the velocity, which in some cases is positive and in other cases negative.

Upstream of the cluster the gas distribution presents a wide lobe, located below its centre and protruding towards the bottom-left corner. This lobe results from the gravitational effect of the central mass condensation of the cluster, which at this time is very dense ($\sim 10^{-16}$ g cm^{-3}, which correspond to 10^6M$_\odot$ pc^{-3}, see Fig. 3), and it can deviate the trajectory of the gas flowing towards it from the back of the tail, along the accretion column and towards the core. In some cases, the flowing gas can move past the centre and orbit around it, thus originating the lobe.

The stellar component in the core appears more diffuse than at 26 Myr, but the mass outside the innermost ~ 3 pc is negligible.

Little differences are visible in the maps computed at 63 Myr, i.e. at the end of the SF. The only remarkable features are the disappearance of the lobes and a more circular distribution of the star particles around the core.

3.2 Evolution of the stellar component

The left column of Fig. 3 shows the density profiles of FG (green dash–dotted lines) and SG (black dashed lines) stars computed at various times, as well as the density profiles of SG stars with different helium abundances. The stellar density profiles are computed assuming an origin placed at the centre of the computational box. In addition to showing the evolutionary path leading to the multiple populations found at the end of our simulations, the panels at different times illustrate the properties of multiple populations if the SG SF episode was truncated at earlier times.

At $t \sim 10$ Myr, all the He-rich SG stars which have purely formed out of the AGB ejecta follow a very steep density profile. At $t = 25.7$ Myr the shock has already crossed the cluster centre, and the central density is slightly larger than the one at $t \sim 10$ Myr. The total density is still dominated by He-rich ($Y > 0.33$) stars, but also stars with a lower He content are present, which have formed after the re-accretion shock has passed through the core. In particular, one SG stellar component with $0.30 < Y \leq 0.33$ is visible and characterized by a flatter density profile. Also another smaller population of stars with $Y < 0.30$ is present, visible at the bottom of the panel. At this time the central density reaches values larger than $> 10^5$ M$_\odot$ pc^{-3}.

Later, at 39.5 Myr, four different populations are present, with different degrees of concentration. Remarkably, the slope of the density profile shows a dependence on the He content: in general, the lower Y values, the flatter the resulting distribution.

At $t = 63.5$ Myr the stars with $0.27 < Y \leq 0.30$ dominate the density distribution practically at all radii, with the exception of the innermost regions (i.e. at radii <0.7 pc) which still sees the predominance of the most He-rich stars.

At all times, in the innermost 2–3 pc the total stellar density is dominated by SG stars, whereas at larger radii it is dominated by FG stars. It is interesting to point out that our simulations predict that the more extreme and less diluted SG population is more spatially concentrated than the more diluted SG stars. A similar trend has been found in the observational study of the spatial distributions
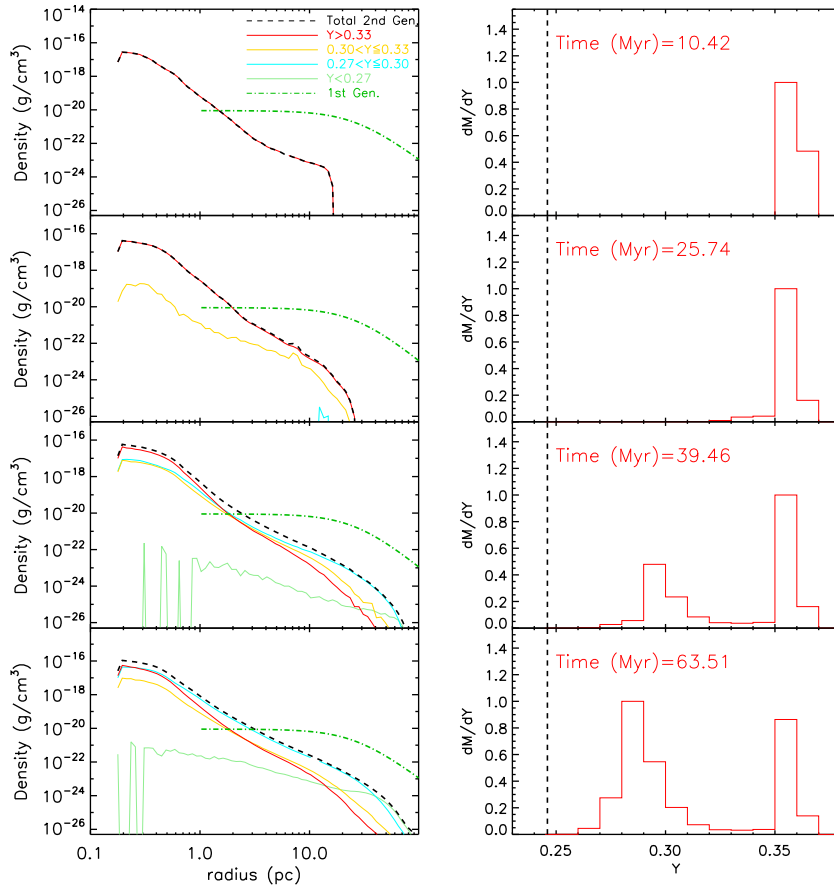
Figure 3. Left column: total density profile for SG stars at various time steps and profiles for stars of different He abundance for our low-density model ($\rho = 10^{-24}$ g cm^{-3}). Also the density profile of FG stars is reported (see the legend in the top-right panel). Right column: distribution of the He mass fraction Y in SG stars at various time steps (indicated in each panel). The distributions have been computed by adding up the total stellar mass in each bin of Y, and then normalizing each distribution to its maximum value. The dashed lines represent the values of FG stars.

of the SG populations in NGC 2808 by Simioni et al. (2016), who showed that the most extreme SG stars are more concentrated than the intermediate SG and the FG populations (see also Johnson & Pilachowski 2012 for a spectroscopic study showing a similar trend in M13). The study of the kinematics of the multiple populations of NGC 2808 (Bellini et al. 2015) also suggests more significant differences between the structural and kinematical properties of the most extreme SG populations and those of the FG and other SG populations. In the future, it will be important to study further the long-term dynamical evolution of systems like those emerging from our simulations and explore the possible dynamical implications of the differences in the chemical abundances of the various SG populations (see e.g. Dalessandro et al. 2018; Fare, Webb & Sills 2018, for the possible differences in the distribution of populations with different helium abundances in dynamically old clusters).

In the right column of Fig. 3 we show the distribution of the helium abundance in SG stars for our low-density model calculated at different times. These panels nicely illustrate the formation history behind the chemical properties of the SG stars. The SG population is initially dominated by the extreme SG forming from undiluted AGB ejecta. As the SG formation proceeds and pristine gas starts to dilute the AGB ejecta, all the panels show the development of extended distributions and the appearence of stars characterized by less extreme chemical abundances. We point out that discrete population groups can emerge also in the case of a

continuous SF as a result of the chemical discontinuity introduced by the infall of pristine gas (see also D'Ercole et al. 2008). It is worth noting that the positions of the two peaks of SG stars are qualitatively in agreement with the ones observed in real clusters such as, e.g. the stellar populations of NGC 2808 (Piotto et al. 2007), in which three distinct populations have been found with Y = 0.248, Y = 0.3, and Y = 0.37 (see also Milone et al. 2015; D'Antona et al. 2016, for the identification of two more populations in NGC 2808 and their possible origin).

3.3 High-density model

In the case of pristine gas with a density 10 times larger ($\rho_{pg} = 10^{-23}$ g cm^{-3}) than that considered in the previous section, the recollapse of the ISM on to the cluster starts earlier than in the low-density case, namely 10 Myr after the end of the explosions of FG type II SNe, or ~1 Myr after the beginning of the AGB phase. This has important consequences on the SF history of SG stars and on their chemical abundance patterns.

In Fig. 4, we show density and temperature maps of our simulation which includes a denser infalling gas in the *x–y* plane computed at 6, 14, 26, and 64 Myr, along with contour maps showing the spatial distribution of SG stars.

It is interesting to point out the significant difference between the structure of the tail and that shown in Fig. 2, in particular the
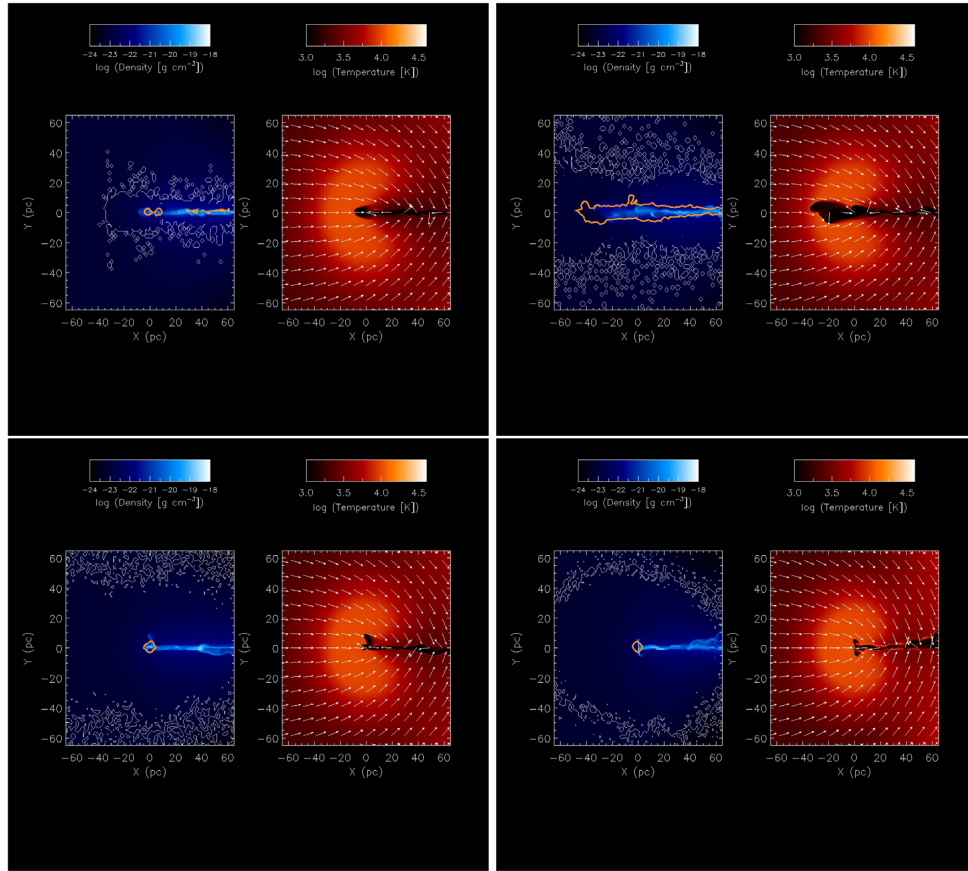
Figure 4. Two-dimensional gas density (left-hand panels of each plot) and temperature (right-hand panels of each plot) maps computed in the *x*–*y* plane for our denser gas simulation at various time steps (from top-left, clockwise: 6, 14, 26, and 64 Myr). The white arrows in the temperature maps represent the velocity field. The white and orange contours describe regions where the SG stellar density is $\geq 10^{-6}$ and ≥ 0.01 times the maximum value, respectively. The orange contours enclose large fractions (> 70 per cent) of the SG stellar mass.

overall inhomogeneous appearance and the presence of various gas condensations visible along the tail. The density and temperature maps at 6 Myr already show the presence of a narrow, cold, dense tail along which various dense knots of gas are recognizable. The larger density of the gas is the cause of a stronger cooling occurring along the stream, which gives rise to a less homogeneous tail than in the previous case and to the development of more prominent condensations which are visible when comparing the density maps of the high-density models with those shown in Fig. 2.

Overall, the distribution of the stars runs along the stream, as outlined by the thin, white contours. In the centre of the density map computed at 6 Myr, two very close, nearly circular stellar condensations are visible (thick orange contours in Fig. 4; see its caption for further details), arising in correspondence of two density enhancements located in the most central region of the plot. Other stellar structures are aligned on the symmetry axis of the plot, lying >20 pc away from the cluster centre. In the temperature map, the motion of the cold gas and its accretion along the tail and on to the cluster is already visible at 6 Myr.

The maps at 14 Myr outline further the various dense gas knots along the stream. Globally, the extent of the stellar structures appears larger than at the previous time; around the central region a couple of lobes of cold gas have developed, extending towards the leftmost boundary and presenting features similar to those already described when we discussed Fig. 2.

As visible in the density map at 26 Myr, the tail appears now more homogeneous than before, and in the cluster centre most of the new stars seem to have settled on to a more regular, circular distribution. The extent and the size of the lobes seem to have reduced with respect to the previous time.

At 64 Myr the stars are scattered all over in the plane, but 90 per cent of the total stellar mass is contained within a very narrow region at the centre of the cluster (orange contour in the density map).

The presence of various stellar condensations located in different regions of the computational volume is confirmed by the stellar density profiles. In the left column of Fig. 5 we show the density profiles of stars of various chemical composition (as traced by their He content) at different times.

As in the previous case, the density profiles have been computed in a reference frame with the origin placed at the centre of the computational grid.

At 6.3 Myr the total SG density profile (black dashed line) presents various peaks associated with some of the substructures visible in Fig. 4.

The distribution of the most He-rich stars presents a peak at <0.5 pc, which coincides with the highest density value of the entire stellar distribution. The inner density profile is dominated by the most He-rich (Y > 0.33) stars, out to radii ∼2 pc. At radii >2 pc, the highest density values are presented by stars with 0.27 < Y < 0.30, which are clustered between 4 and ∼5 pc, as also visible
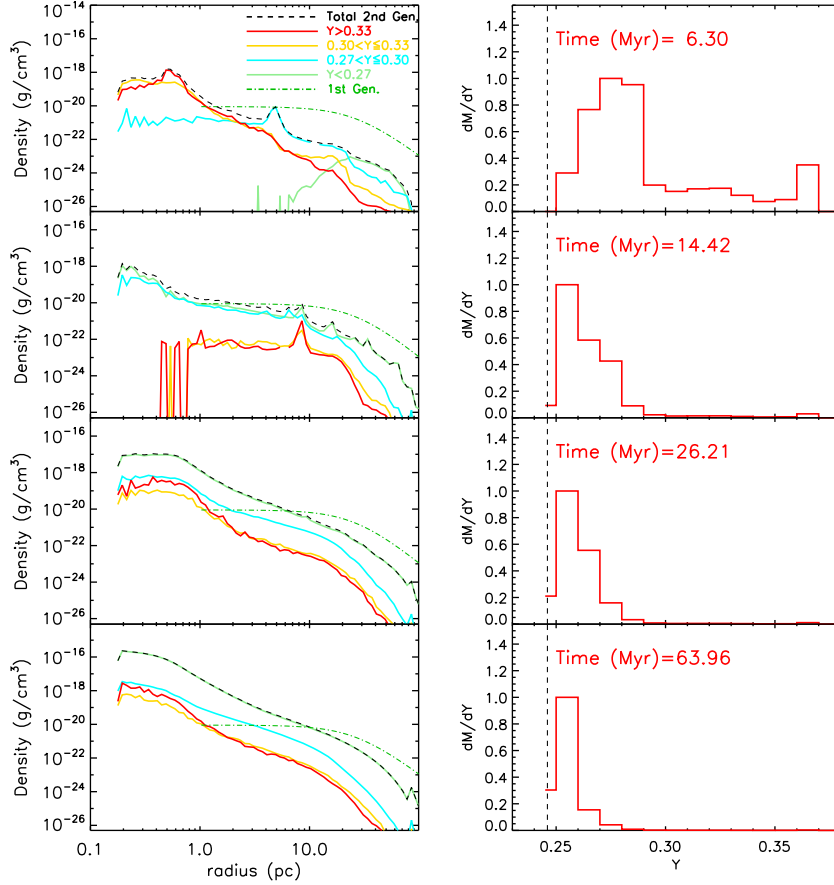
Figure 5. Left column: density profiles of SG stars in our denser model ($\rho = 10^{-23}$ g cm^{-3}) at various time steps. Right column: He mass distribution in SG stars at different times. Lines are as in Fig. 3.

from the secondary peak of the total density profile at this radius. Other two substructures composed of stars with $0.3 < Y \leq 0.33$ and $Y < 0.27$ are visible at 20 pc and at radii >40 pc, respectively. The component with the lowest He content dominates the total SG profile at radii >30 pc.

In the SG density profile computed at 14.4 Myr the secondary peaks due to the stellar populations born with different compositions are still partially visible.

At this time, the two less He-enhanced components contribute similarly to the density profile at radii between 0.5 and 10 pc, with a slight predominance of stars with $Y < 0.27$, which tend to dominate the total SG mass distribution practically at all radii.

A few distinct, minor peaks are visible in the density profiles of the subpopulations, such as one of the most He-rich stars at $\sim$7 pc. The stellar density distributions of the most He-rich components are flatter than the ones seen at 6 Myr.

At $t = 26$ Myr the density profiles appear smoother than at previous times, as they have basically lost their original multipeaked character. As seen earlier, at this time the bulk of the stellar component appears regular in shape and occupies the centre of the cluster. The bulk of the most He-rich stars occupies the innermost 1 pc. However, at all radii the SG mass is dominated by the stars with $Y < 0.27$.

These are the main properties of the SG subsystem also at subsequent times, as confirmed by the density profile computed at the end of the SF episode ($t = 64$ Myr).

The He mass distributions in SG stars and in the denser model are shown in the right column of Fig. 5, and they show marked differences with respect to the lower density model.

Also in this case, the panels of Fig. 5 are calculated at various evolutionary times and besides showing the SG formation history, they also allow us to characterize the properties of the SG if SFs stopped before $\sim$65 Myr.

A large separation between the two newly born populations is visible from the the Y distributions calculated at 6 Myr. The relative heights of the peaks of these two populations appear reversed with respect to the case of the low-density model soon after the beginning of the pristine-gas dilution, in that the stars with large ($Y\sim 0.35$) values are subdominant with respect to SG stars with $Y\sim 0.27$.

At later times, the Y distribution shows a progressive thickening of the less extreme, low-He peak (more similar to the Y value of FG stars) and a substantial disappearance of the peak of the stars with the highest Y values.

It is interesting to point out that the rapid infall of pristine gas leads to an SG population dominated by stars with very modest helium enhancement.

Finally, an interesting point to discuss concerns the chemical composition of SG stars during the earliest stage of SG formation. Our results show that at 6 Myr two chemically distinct populations have already formed: a first one rich in He and a second one characterized by Y values which are intermediate between the most
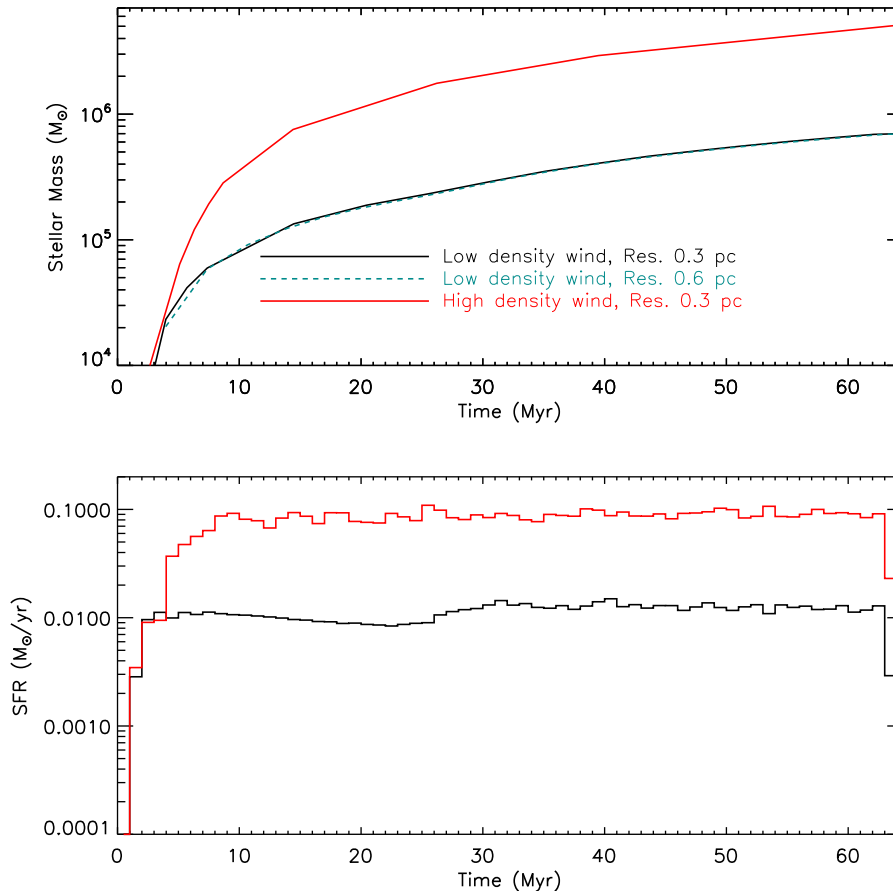
Figure 6. Upper panel: evolution of the SG stellar mass in our simulations. The black solid line and the cyan dashed line are the results for the low-density model at high and low resolution, respectively. The red solid line shows the results in the case of the denser model. Lower panel: SF histories of our low-density and high-density models. The black (red) thin solid line is the SF rate as a function of time for our low- (high-)density model.

He-rich SG stars and those of FG stars. In terms of mass, it is this second new population which represents the vast majority of the SG stars. Our results thus indicate that it is possible to have a population with chemical features similar to those of the FG, but formed more than 40 Myr later, i.e. soon after FG AGB stars start to shed their ejecta. The age difference between the latter and the first enriched SG stars made of pure AGB ejecta could be much lower, in this case of the order of 6 Myr. Depending on the fraction of FG stars remaining in the cluster, this could complicate the interpretation of observational estimates of age differences in multiple stellar populations and potentially provide misleading constraints for theoretical models.

4 DISCUSSION

Our simulations have clearly shown how a compact SG subsystem can form in the inner regions of an FG cluster out of the ejecta of AGB stars along with pristine gas accreted from an external reservoir. The hydrodynamical simulations presented here model in detail the dynamics of AGB ejecta and that of the infalling pristine gas; our results show that the amount of pristine gas re-accreted and mixed with the AGB ejecta lead to chemical properties in agreement with the main abundance patterns observed in Galactic GCs. The total stellar mass at the end of our simulations amounts to 7×10^5 $M_\odot$ for our low-density model, and to $\sim 5 \times 10^6$ $M_\odot$ for the denser model (upper panel of Fig. 6).

Considering that the total initial FG mass in the computational box is 9×10^6 $M_\odot$, the ratio of the total initial FG to the total SG mass formed in the two cases is about 12.9 for the low-density model and 1.8 for the high-density model. Considering also that the code does not allow more than 90 per cent of the gas in each cell to be used for SF, thus limiting the amount of gas converted in stars as discussed in Section 2.2.2, these ratios could be slightly smaller, possibly by a factor ~ 0.9 (although, owing to the stochasticity of SF, it is not possible to quantify in detail this effect). Although detailed studies of the dynamical evolution of these models are necessary, these results imply that the FG mass-loss required to produce FG-to-SG mass ratios similar to those observed in old GCs is significantly less extreme than that often reported in the literature (suggesting mass-loss factors up to 100 or more and referred to as the mass budget problem) and more in line with factors of the order of $\sim$5–10, already suggested by previous studies which took into account the contribution of both AGB ejecta and the diluting pristine gas (see e.g. D'Antona et al. 2013; Ventura et al. 2014).

In Fig. 6 we also show the stellar mass as a function of time computed in the low-density model at lower resolution (0.6 pc). Even if we do not resolve the Jeans scale (as this would require prohibitive computational resources), the comparison between the results in the low-density model at different resolution indicates that in our simulation numerical convergence is satisfactory.

4.1 On massive stars in the second generation

In our model, an efficient gas accretion and a prolonged SF history (shown in the lower panel of Fig. 6) are possible only by neglecting the feedback of stellar winds and SNII from SG massive stars (i.e. those with $M > 8\ \mathrm{M_\odot}$), which could in principle hamper mass accretion on to the cluster (Matzner & Jumper 2015) and, under certain conditions, even cause the immediate end of SF (see D'Ercole et al. 2008, also for the possible role of other feedback sources). In addition, should a significant fraction of SNII ejecta be retained in the cluster they could produce a spread in, for example, Fe which is found only in a subset of the sample of Galactic clusters studied so far (see e.g. Renzini et al. 2015; Da Costa 2016, and references therein). The possible role of SNe in the origin of the more complex manifestations of multiple populations such as the multiple populations in NGC 2808 has also been discussed by D'Antona et al. (2016).

A detailed study of the possible role of massive stars in the dynamics of the gas during SG SF and the implications for the resulting SG chemical properties requires additional simulations and further study beyond the scope of this investigation.

Here however we discuss and review a few solutions and interesting possibilities concerning the role of massive stars in the formation of the SG population.

A possibility raised in a few previous studies (see e.g. Decressin et al. 2007; D'Ercole et al. 2008, 2010) is that the stellar IMF of the SG is truncated at masses smaller than $M \sim 8$–$10\ \mathrm{M_\odot}$. As previously pointed out in the literature (see e.g. Renzini et al. 2015), the process of SF in a pre-existing crowded stellar environment is unexplored and it is unclear whether and how the extreme environment of SG formation can affect the IMF of the SG. Very recently, by means of non-turbulent smoothed particle hydrodynamics simulations, Bekki (2019) showed that the growth of large, high-density gas clumps that lead to the formation of massive stars with $M > 8\ \mathrm{M_\odot}$ can be severely suppressed in GCs. Further studies on both theoretical and observational sides will be needed to confirm this result and shed more light on the IMF of multiple populations in GCs.

Another interesting possibility is opened by the extremely compact structure of the SG subsystem emerging from the simulations presented in this paper. Such an SG subsystem is characterized by a half-mass radius equal to 0.4 pc in the low-density model and of 3 pc in the high-density model, with a total mass of $\gtrsim 10^6\ \mathrm{M_\odot}$. In such a compact and high-density SG subsystems, if massive stars form, they are likely to be significantly affected by close encounters and physical collisions with other SG stars. In the case of the more compact SG subsystem emerging from our simulations, massive stars could rapidly segregate in the inner regions and populate an even denser subcomponent before they can evolve and explode as SNII.

As for the high-density model, it is interesting to point out its complex structure during the very early stages of SG formation, characterized by a pronounced tail and several small and dense clumps eventually merging to form the final SG subsystem (see e.g. McMillan, Vesperini & Portegies Zwart 2007, for a discussion of the early dynamics and mass segregation in clumpy systems).

All the aspects concerning the dynamical evolution and the possible collisional history of massive stars in SG subsystems will require specific simulations which we defer to a future study; here, however, it is worth mentioning that an interesting possibility in the context of studies of multiple-population cluster formation has been proposed by Sills & Glebbeek (2010), who suggested that

massive star collisions (even though in their work the massive stars considered belonged to the FG population) might release processed gas out of which SG stars would form. In the context of our model, additional gas for the SG formation might therefore be provided by the physical collisions of the massive SG stars themselves. In a future study on the early dynamics of the SG subsystem we will further explore also this aspect.

4.2 On the detectability of globular clusters during SG star formation

In our model, the SG forms at the centre of the FG cluster (for a detailed study of the detectability of GCs during FG SF, see Pozzetti, Maraston & Renzini 2019) as an extremely compact and dense stellar subsystem surrounded by a more spatially extended FG component. Under these conditions, during the SG formation the cluster should be composed of a faint and nucleated core, possibly surrounded by a diffuse component. If the SG contains a few massive stars, they should be visible before possibly undergoing the rapid sequence of collisions facilitated by the cluster dense environment, as discussed in the previous subsection. As new massive stars (MS) form and before suffering collisions with other massive stars, during their drift towards the very centre they should emit UV light. To estimate the UV magnitude associated with massive stars in the SG subsystem, one could assume that the most massive stars with mass $M > M_{\mathrm{dis}}$ disappear as they are rapidly affected by collisions in the centre, and that new MS are continuously formed.

In such a case, we can perform an attempt to estimate the apparent magnitude of the cluster by means of the spectrophotometric code STARBURST99 (Leitherer et al. 2014) and assuming a truncated IMF. For this computation, we consider the redshift range probed by the MUSE instrument (Bacon et al. 2017), mounted on the Very Large Telescope, and its detected Lyman α emitters ($3 \leq z \leq 6.7$; e.g. Inami et al. 2017). This instrument has allowed considerable steps forward in the identification of extremely faint sources at high z, in particular in gravitationally lensed fields (Karman et al. 2017; Vanzella et al. 2017a, b; Mahler et al. 2018).

When SG stars start to form, we have a $10^7\ \mathrm{M_\odot}$ FG which is already 30 Myr old, which we assume have originated in an instantaneous burst.

To compute the magnitudes, we have considered the SF histories shown in the bottom panel of Fig. 6 and two different IMFs: the Salpeter (1955) IMF, characterized by a power law with exponent $\alpha = 2.35$, and a steeper IMF with $\alpha = 3.3$, representative of an SG deprived in massive stars. With these ingredients, we can compute the evolution of the 1500 Å apparent magnitudes of the cluster in all of its components (FG and SG) in the low-density and high-density models, as shown in Fig. 7. In this case, for the computation of the apparent magnitudes the cluster has been placed to $z = 6$. In the low-density model, SG stars are always fainter than FG stars. In the case of a Salpeter IMF, due to the effect of SG stars at the peak of their luminosity, occurring at ~ 60 Myr, the cluster is less than one magnitude brighter than the FG component. On the other hand, in the denser model the luminosity of the cluster is dominated by SG stars already after a few Myr in the case of a Salpeter IMF, and after 60 Myr in the case of a steeper IMF. Even in the case of the low-density model, the cluster presents magnitudes not far from those already accessible in current observational samples, in particular in lensed fields (Vanzella et al. 2017a). Very recently, Vanzella et al. (2019) reported on a superdense and compact star-forming region at $z = 6.143$, with an effective radius of 13 pc (with F105W magnitude of 31.1), embedded in a more diffuse, larger structure of a size of
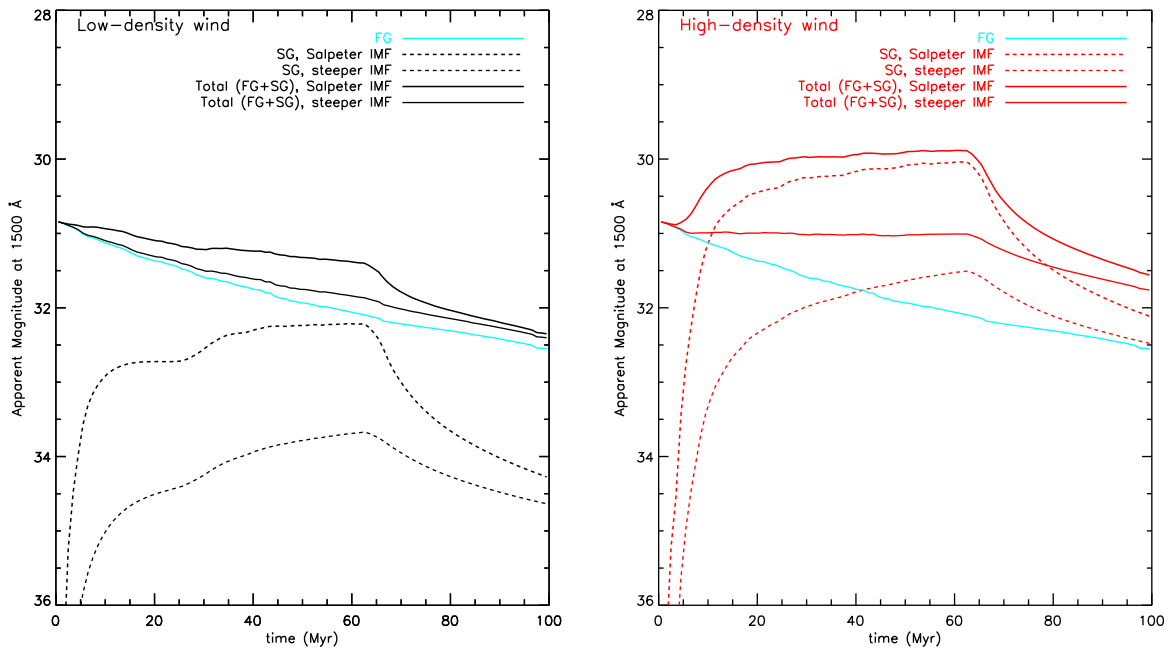
Figure 7. Evolution of the apparent magnitude at 1500 Å of FG and SG stars in the low-density (left-hand panel) and high-density (right-hand panel) model, calculated assuming a cluster placed at $z = 6$. In each panel, the thick cyan line is the magnitude calculated for FG stars. The thick solid and thick dashed black (red) lines are the apparent magnitudes of the entire cluster (including FG and SG stars) and of the SG computed with STARBURST99 assuming a Salpeter IMF in the low-density (high-density) model. The thin solid and thin dashed black (red) lines are the magnitudes of the entire cluster and of SG stars, respectively, computed assuming a steeper IMF, characterized by a slope $\alpha = 3.3$, in the low-density (high-density) model.

~ 40 pc (see also Bouwens et al. 2017). This object is part of a larger structure, which contains several distinct, tiny sources, with magnitudes between 29.6 and >32, and distributed across a region which extends for several tens kpc.

These observational studies show that the detection of young GCs are highly facilitated when they are located in lensed fields, in particular in strongly magnified regions, where very faint magnitudes and small scales can be probed, with good control of the systematics (Vanzella et al. 2017a, b). In such generally narrow regions, the magnification due to strong lensing can reach extremely high values ($\mu > 10$, see Vanzella et al. 2017a, b) and the magnitudes are boosted by $2.5 \log 10(\mu)$.

The appearance of the system would be significantly dependent also on its dynamical evolution. If a significant fraction of the FG had expanded, in principle it could be possible to detect the SG as a faint point-like source surrounded by a diffuse component.

Observationally, the scales of the SG will be addressable in the future due to the ESO Extremely Large Telescope which, if exploited in lensed fields, will allow us to spatially resolve systems of ~ 2 pc at $z > 3$ and down to very faint magnitudes, (>32, Fiorentino et al. 2017).

Other considerations related to the environment of these objects are in order. In principle, one could also expect the high-redshift precursors of GCs to be clustered at their birth as in the local Universe (Kravtsov & Gnedin 2005; Renzini 2017), i.e. to be aggregated into groups of newly formed systems. This seems to be confirmed by a new study of star-forming complexes in a lensed field at $z \sim 6$, which has shown the presence of a handful of very faint sources lying within a group of approximate size of less than 10 arcsec, corresponding to ~ 60 kpc (Vanzella et al. 2019).

These system are also expected to be surrounded by a large reservoir of cold gas, perhaps visible as a diffuse Lyman α component. In fact, due to its resonant nature, the Ly α transition

is an extremely powerful tracer of the structure of the neutral gas located around stellar structures (e.g. Gronke et al. 2017).

A large reservoir of dense, cold gas is required to fuel further SF episodes, and it has to be readily available near the systems (D'Ercole et al. 2016). If present in large amount and dense enough, this reservoir of cold gas could also be detected by means of strong infrared lines, such as the [CII]158 μm fine structure line, a very efficient and dominating coolant for neutral gas.

4.3 Future directions

Beside investigating further the structural parameters of the cluster and the ones related to the properties of the external environment, in the future it will be important to extend this study to explore other scenarios proposed for multiple populations in GCs.

So far, the origin of multiple populations has generally not been addressed in hydrodynamical simulations of GC formation (e.g. Nakasato, Mori & Nomoto 2000; Fujii & Portegies Zwart 2016). One exception is the study of Howard et al. (2019), which use 3D radiative hydrodynamics simulations to study the formation of young massive clusters and their subsequent evolution for 5 Myr.

It will be important to exploit such models to study the SF and the dynamical evolution of young clusters for more extended evolutionary times. Currently, this is computationally challenging for a number of reasons. One difficulty is represented by the necessity to include massive stellar feedback, in both pre-SN and SN phases. Previous studies have shown that the energetic feedback of MS can accelerate their ejecta and the surrounding gas to very high velocities (> 1000 km s^{-1}), which can lead to extremely short computational time steps, which are necessary to satisfy the Courant–Friedrichs–Lewy condition (Emerick, Bryan & Mac Low 2019; Romano et al. 2019). Moreover, the dynamical evolution of massive stars need to be treated by means of direct N-body

simulations, which are generally problematic for large number of particles ($> 500\,000$ stars, Heggie 2014). Steps forward are currently being attempted with new parallel computing technologies (e.g. GPUs) for *N*-body studies, but the problem of the coupling with hydrodynamics is still to be tackled.

To test scenarios such as the one of massive (Elmegreen 2017) and supermassive stars (Gieles et al. 2018), more physical ingredients will need to be included in hydrodynamical simulations, including fully collisional *N*-body dynamics. A new numerical method to resolve the dynamics of the stars and gas which include coupling of hydrodynamic codes, an *N*-body code, and a stellar evolution code is the Astro-physical MUlti-purpose Software Environment (AMUSE, Pelupessy et al. 2013; Portegies Zwart & McMillan 2018). Recently, Wall et al. (2019) presented an interface for the FLASH hydrocode in the AMUSE framework. Such a work will be a reference for any future attempt to model multiple populations in young stellar clusters with hydrodynamic codes in various scenarios.

5 CONCLUSIONS

In this paper we have used grid-based, three-dimensional hydrodynamical simulations to model the formation of SG stars in a massive cluster moving through a uniform background gas distribution. After the explosion of all FG type II SNe, when the cluster is about 40 Myr old, SG stars start to form out of the ejecta of AGB stars and external gas with pristine (i.e. same as FG stars) composition accreted from the environment in which it is moving. The epoch of formation of SG stars is assumed to last about 60 Myr, until the cluster is ∼100 Myr old. Our study is focused on a massive cluster with an initial FG mass equal to $10^7\,M_\odot$, ($9 \times 10^6\,M_\odot$ inside the computational box considered in our hydrosimulations) a possible progenitor of the most massive clusters in the old Galactic GC population. We do not model the formation of FG stars and assume a cluster already in place, and that at an age of 40 Myr all the primordial gas and the FG type II SNe ejecta have been expelled. The occurrence of type II SNe has left the cluster in an extended cavity, which is then replenished by the later recollapse of the interstellar gas on to the cluster. We have considered two different values for the density of the background pristine gas, a low-density case with $\rho = 10^{-24}\,\mathrm{g\,cm^{-3}}$ and a high-density one with $\rho = 10^{-23}\,\mathrm{g\,cm^{-3}}$. These two choices lead to different infall times, with important implications for the resulting chemical abundance pattern of the SG population. Although some of the conditions chosen for our model are idealized, the physical parameters chosen for the inflowing matter have been selected in order to describe gas densities observed in real systems and expected to be typical for star-forming galaxies at high redshift. Our main results can be summarized as follows:

(i) In the low-density model, a very compact, dense SG stellar subsystem starts to form at the cluster centre immediately at the beginning of our simulation from the undiluted ejecta of the most massive AGB stars. The low density of the external gas causes the recollapse of the gas in the cavity, and the resulting dilution, to impact on the centre of the cluster approximately 20–25 Myr after the onset of SF. After this time, the interstellar gas flows towards the centre of the system mostly through an accretion column, which has emerged soon after a turbulent tail aligned with the axis of motion was formed. The SG formed in this simulation is characterized by two distinct groups: one with strong helium enhancement formed from undiluted AGB ejecta and one with more moderate helium enhancement formed later in the SG SF event from AGB ejecta diluted with pristine gas.

(ii) In the denser gas model, the pristine gas infall is more rapid and therefore the dilution of the AGB ejecta forming SG stars starts earlier. This implies that the SG population is dominated by stars with less extreme chemical anomalies, as traced by the He abundances of SG stars and as observed in many Galactic GCs. In this case the tail along which gas can be accreted presents a more clumpy structure, and in correspondence of the clumps new separate stellar aggregates can form, located in different positions in the computational volume. Approximately 26 Myr after the start of the SG SF the morphology of the cluster appears more regular and approximately spherical. Also in this case, the SG subsystem is concentrated in the innermost regions of the cluster.

(iii) We find that the first and most helium-enhanced SG stars are more centrally concentrated than SG stars born later and with less extreme He content. This trend is consistent with a few studies in which the spatial distribution of the different SG subpopulations was investigated (see Johnson & Pilachowski 2012; e.g. Simioni et al. 2016).

(iv) In the two models presented here, at the end of the SG formation the ratio of the initial mass in FG stars to that in SG stars is equal to about 1.8 for the high-density model and about 12.8 for the low-density model. Although these values are larger than the observed present-day values of this ratio (see e.g. Milone et al. 2017) and require a subsequent preferential loss of FG stars, such a required FG mass-loss is significantly less extreme than that often reported in the literature. Previous studies have explored the possible dynamical paths leading to the needed loss of FG stars during the cluster early and long-term dynamical evolution (see e.g. D'Ercole et al. 2008) and we will further extend the study of this dynamical aspect in future investigations.

(v) In both models presented here, already after 10–20 Myr the SG subsystem is very compact and characterized by a high central density ($> 10^5\,M_\odot\,\mathrm{pc}^{-3}$). Although further studies to explore in detail the early and long-term dynamics of the SG subsystem are necessary, we pointed out that the high density of the SG subsystem found in our simulations may lead to rapid and numerous physical collisions between massive SG stars before they explode as SNII. An interesting consequence of these collisions might be the stripping of the stars' outer layers possibly providing additional gas for the formation of SG stars.

(vi) By means of the STARBURST99 code, we have computed the expected apparent magnitude of the simulated cluster, assuming that it is placed at $z = 6$, as some recently discovered high-redshift young stellar clusters, accessible due to the MUSE instrument. We have tested two different choices for the stellar IMF, including a standard, Salpeter (1955) power-law IMF and a steeper IMF, representative of an SG deprived in massive stars.
Even in the most conservative, low-density model, the cluster presents UV magnitudes between ∼31 and 32, not far from those already observationally accessible in lensed fields (Vanzella et al. 2019).

In the future, we plan to extend the study presented here with a survey of simulations aimed at exploring the SG formation in clusters with a broader range of different structural parameters and at following their subsequent early and long-term dynamical evolution. The analysis presented here is conducted in the AGB scenario proposed by D'Ercole et al. (2008). Of course, all the other proposed models might lead to a different evolution of the chemical and structural properties of GCs. The extension of the simulations presented here to these scenarios will be therefore valuable to allow

a better discrimination between various hypotheses proposed so far for the formation of GCs.

REFERENCES

Bacon R. et al., 2017, A&A, 608, A1

Bastian N., Cabrera-Ziri I., Salaris M., 2015, MNRAS, 449, 3333

Bastian N., Lardo C., 2018, ARA&A, 56, 83

Bedin L. R., Piotto G., Anderson J., Cassisi S., King I. R., Momany Y., Carraro G., 2004, ApJ, 605, L125

Bekki K., 2019, MNRAS, 486, 2570

Bekki K., Mackey A. D., 2009, MNRAS, 394, 124

Bellini A., Piotto G., Bedin L. R., King I. R., Anderson J., Milone A. P., Momany Y., 2009, A&A, 507, 1393

Bellini A. et al., 2015, ApJ, 810, L13

Bondi H., 1952, MNRAS, 112, 195

Bondi H., Hoyle F., 1944, MNRAS, 104, 273

Bouwens R. J., Illingworth G. D., Oesch P. A., Maseda M., Ribeiro B., Stefanon M., Lam D., 2017, preprint (arXiv:1711.02090)

Breen P. G., 2018, MNRAS, 481, L110

Calura F., Pipino A., Chiappini C., Matteucci F., Maiolino R., 2009, A&A, 504, 373

Calura F., Few C. G., Romano D., D'Ercole A., 2015, ApJ, 814, L14

Carretta E. et al., 2009a, A&A, 505, 117

Carretta E., Bragaglia A., Gratton R., Lucatello S., 2009b, A&A, 505, 139

Chabrier G., 2003, PASP, 115, 763

Ciotti L., D'Ercole A., Pellegrini S., Renzini A., 1991, ApJ, 376, 380

Conroy C., Spergel D. N., 2011, ApJ, 726, 36

D'Antona F., Caloi V., D'Ercole A., Tailo M., Vesperini E., Ventura P., Di Criscienzo M., 2013, MNRAS, 434, 1138

D'Antona F., Vesperini E., D'Ercole A., Ventura P., Milone A. P., Marino A. F., Tailo M., 2016, MNRAS, 458, 2122

D'Antona F., Ventura P., Marino A., Milone A. P., Tailo M., Di Criscienzo M., Vesperini E., 2019, ApJ, 871, L19

D'Ercole A., Vesperini E., D'Antona F., McMillan S. L. W., Recchi S., 2008, MNRAS, 391, 825

D'Ercole A., D'Antona F., Ventura P., Vesperini E., McMillan S. L. W., 2010, MNRAS, 407, 854

D'Ercole A., D'Antona F., Vesperini E., 2011, MNRAS, 415, 1304

D'Ercole A., D'Antona F., Carini R., Vesperini E., Ventura P., 2012, MNRAS, 423, 1521

D'Ercole A., D'Antona F., Vesperini E., 2016, MNRAS, 461, 4088

da Costa G. S., 2016 , in Bragaglia A., Arnaboldi M., Rejkuba M., Romano D., eds, Proc. IAU Symp, Vol. 317. The General Assembly of Galaxy Halos: Structure, Origin and Evolution. Kluwer, Dordrecht, p. 110

Dalessandro E. et al., 2018, ApJ, 859, 15

de Mink S. E., Pols O. R., Langer N., Izzard R. G., 2009, A&A, 507, L1

Decressin T., Meynet G., Charbonnel C., Prantzos N., Ekström S., 2007, A&A, 464, 1029

Dejonghe H., 1987, MNRAS, 224, 13

Denissenkov P. A., Hartwick F. D. A., 2014, MNRAS, 437, L21

Denissenkov P. A., VandenBerg D. A., Hartwick F. D. A., Herwig F., Weiss A., Paxton B., 2015, MNRAS, 448, 3314

El-Badry K., Wetzel A., Geha M., Hopkins P. F., Kereš D., Chan T. K., Faucher-Giguère C.-A., 2016, ApJ, 820, 131

Elmegreen B. G., 2017, ApJ, 836, 80

Emerick A., Bryan G. L., Mac Low M.-M., 2019, MNRAS, 482, 1304

Fare A., Webb J. J., Sills A., 2018, MNRAS, 481, 3027

Ferland G. J., Korista K. T., Verner D. A., Ferguson J. W., Kingdon J. B., Verner E. M., 1998, PASP, 110, 761

Ferraro F. R., Sollima A., Pancino E., Bellazzini M., Straniero O., Origlia L., Cool A. M., 2004, ApJ, 603, L81

Few C. G., Courty S., Gibson B. K., Michel-Dansac L., Calura F., 2014, MNRAS, 444, 3845

Fiorentino G. et al., 2017, MAORY science cases white book. preprint (arXiv:1712.04222)

Fujii M. S., Portegies Zwart S., 2016, ApJ, 817, 4

Gieles M. et al., 2018, MNRAS, 478, 2461

Goodman M., Bekki K., 2018, MNRAS, 478, 3564

Gratton R. G., Carretta E., 2010, A&A, 521, A54

Gratton R., Sneden C., Carretta E., 2004, ARA&A, 42, 385

Gratton R. G., Carretta E., Bragaglia A., 2012, A&AR, 20, 50

Gronke M., Dijkstra M., McCourt M., Peng Oh S., 2017, A&A, 607, A71

Haffner L. M. et al., 2009, Rev. Mod. Phys., 81, 969

Heggie D. C., 2014, MNRAS, 445, 3435

Howard C. S., Pudritz R. E., Sills A., Harris W. E., 2019, MNRAS, 486, 1146

Inami H. et al., 2017, A&A, 608, A2

Johnson C. I., Pilachowski C. A., 2012, ApJ, 754, L38

Kaaz N., Antoni A., Ramirez-Ruiz E., 2019, ApJ, 876, 142

Karman W. et al., 2017, A&A, 599, A28

Kravtsov A. V., Gnedin O. Y., 2005, ApJ, 623, 650

Kroupa P., 2001, MNRAS, 322, 231

Kruijssen J. M. D., 2015, MNRAS, 454, 1658

Lardo C., Bellazzini M., Pancino E., Carretta E., Bragaglia A., Dalessandro E., 2011, A&A, 525, A114

Lee Y.-W., Joo J.-M., Sohn Y.-J., Rey S.-C., Lee H.-C., Walker A. R., 1999, Nature, 402, 55

Leitherer C., Ekström S., Meynet G., Schaerer D., Agienko K. B., Levesque E. M., 2014, ApJS, 212, 14

Lin D. N. C., Murray S. D., 2007, ApJ, 661, 779

Mahler G. et al., 2018, MNRAS, 473, 663

Mannucci, Della Valle, Panagia, 2006, MNRAS, 370, 773

Maoz D., Mannucci F., Nelemans G., 2014, ARA&A, 52, 107

Marcolini A., Brighenti F., D'Ercole A., 2003, MNRAS, 345, 1329

Marino A. F., Villanova S., Piotto G., Milone A. P., Momany Y., Bedin L. R., Medling A. M., 2008, A&A, 490, 625

Matzner C. D., Jumper P. H., 2015, ApJ, 815, 68

McMillan S. L. W., Vesperini E., Portegies Zwart S. F., 2007, ApJ, 655, L45

Milone A. P. et al., 2012, ApJ, 744, 58

Milone A. P. et al., 2015, ApJ, 808, 51

Milone A. P. et al., 2017, MNRAS, 464, 3636

Moeckel N., Troop H. B., 2009, ApJ, 707, 268

Mori M., Burkert A., 2000, ApJ, 538, 559

Naiman J. P., Ramirez-Ruiz E., Lin D. N. C., 2011, ApJ, 735, 25

Nakasato N., Mori M., Nomoto K., 2000, ApJ, 535, 776

Park K., Bogdanović T., 2017, ApJ, 838, 103

Pelupessy F. I., van Elteren A., de Vries N., McMillan S. L. W., Drost N., Portegies Zwart S. F., 2013, A&A, 557, A84

Pflamm-Altenburg J., Kroupa P., 2009, MNRAS, 397, 488

Piotto G. et al., 2005, ApJ, 621, 777

Piotto G. et al., 2007, ApJ, 661, L53

Piotto G. et al., 2015, AJ, 149, 91

Plummer H. C., 1911, MNRAS, 71, 460

Portegies Zwart S., McMillan S., 2018, Astrophysical Recipes: The Art of AMUSE. AAS IOP Astronomy, IOP ebooks, Bristol, UK

Pozzetti L., Maraston C., Renzini A., 2019, MNRAS, 485, 5861

Rasera Y., Teyssier R., 2006, A&A, 445, 1

Renzini A., 2017, MNRAS, 469, L63
Renzini A. et al., 2015, MNRAS, 454, 4197
Romano D., Calura F., D'Ercole A., Few C. G., 2019, A&A, preprint (arXiv: 1909.02329)
Rosen A., Bregman J. N., 1995, ApJ, 440, 634
Salpeter E. E., 1955, ApJ, 121, 161
Schmidt M., 1959, ApJ, 129, 243
Shima E., Matsuda T., Takeda H., Sawada K., 1985, MNRAS, 217, 367
Siess L., 2010, A&A, 512, A10
Sills A., Glebbeek E., 2010, MNRAS, 407, 277
Simioni M., Milone A. P., Bedin L. R., Aparicio A., Piotto G., Vesperini E., Hong J., 2016, MNRAS, 463, 449
Sollima A., Ferraro F. R., Bellazzini M., Origlia L., Straniero O., Pancino E., 2007, ApJ, 654, 915
Sutherland R. S., Dopita M. A., 1993, ApJS, 88, 253
Teyssier R., 2002, A&A, 385, 337

Truelove J. K., Klein R. I., McKee C. F., Holliman J. H., Howell L. H., Greenough J. A., 1997, ApJ, 489, L179
Vanzella E. et al., 2017a, MNRAS, 467, 4304
Vanzella E. et al., 2017b, ApJ, 842, 47
Vanzella E. et al., 2019, MNRAS, 483, 3618
Ventura P., D'Antona F., 2011, MNRAS, 410, 2760
Ventura P., di Criscienzo M., D'Antona F., Vesperini E., Tailo M., Dell'Agli F., D'Ercole A., 2014, MNRAS, 437, 3274
Wall J. E., McMillan S. L. W., Mac Low M.-M., Klessen R. S., Portegies Zwart S., 2019, preprint (arXiv:1901.01132)
Wang X. et al., 2019, ApJ, 882, 94
Wardlow J. L. et al., 2017, ApJ, 837, 12

This paper has been typeset from a TEX/LATEX file prepared by the author.